A study of earthquakes along the Mid-Atlantic Ridge between Charlie-Gibbs and the Azores

Hörður Bjarni Harðarson

Faculty of Geoscience
University of Iceland
2015

A study of earthquakes along the Mid-Atlantic Ridge between Charlie-Gibbs and the Azores

Hörður Bjarni Harðarson

10 ECTS thesis submitted in partial fulfillment of a
Baccalaureum Scientiarum degree in Geology

Advisor
Páll Einarsson

Faculty of Geoscience
School of Engineering and Natural Sciences
University of Iceland
Reykjavík, October 2016

A study of earthquakes along the Mid-Atlantic Ridge between Charlie-Gibbs and the Azores
10 ECTS thesis submitted in partial fulfillment of a B.Sc. degree in Geology

Faculty of Geoscience
School of Engineering and Natural Sciences
University of Iceland
Iceland

Abstract

This thesis gives a seismicity overview of the Mid-Atlantic Ridge between the Charlie-Gibbs Fracture Zone and the Azores during the period of 1955-2015. The fault plane solutions on the ridge mostly show normal faulting which is to be expected on a spreading ridge. A few earthquakes produced reverse or transform faulting, the ones occurring close to the axis coincided with transforms on the ridge. Intraplate events are relatively common, showing mostly reverse faulting. The earthquakes follow the axis quite uniformly, the northern part showing a more diffuse nature, the middle following the axis whereas the southern part shows some signs of diffusion. On several locations the activity decreased considerably showing very few or no events. The most prominent around 42°N and 41°N along with 50.5°N, 49°N, 48.5°N, 44°N, 44.8°N and 44.2°N. A zone of increased activity can be seen around 45°N. A total number of 27 sequences were recorded, the five largest with close proximity with transform faults showing a possible link thereof. A Gutenberg-Richter value of 1.74 calculated for the ridge is close to expected values for a spreading ridge. Examining the seismic moment reveals an increase towards the south, peaking at around 43°N, plummeting thereafter and continually rising again towards the south. Spreading rates and azimuth calculated for the ridge are in unison with previous findings with values between 22.21-23.96 mm/year, the azimuth changing (north-south) from 91.23° to 91.02°.

Útdráttur

Þessi ritgerð veitir yfirlit yfir skjálftavirkni á Miðatlantshafshryggnum á milli Charlie-Gibbs þverbrotabeltisins og Azoraeyja á tímabilinu 1955-2015. Brotlausnir á hryggnum sýna að mestu leiti siggengislausnir sem við má búast á fráreksbelti. Nokkrir skjálftar sýndu samgengis- eða þverbrotalausnir, skjálftarnir sem áttu sér stað á eða við hrygginn voru yfirleitt í nálægð við þvergengi. Innanflekaskjálftar voru nokkuð algengir og sýndu að mestu samgengislausnir. Skjálftarnir fylgja hryggnum nokkuð vel þar sem nyrsti hlutinn virðist dreifðari ásamt minna dreifðum syðri hluta. Miðhlutinn er þéttastur og sýnir mestu fylgni við hrygginn. Nokkrar staðsetningar á hryggnum sýna lægðir í skjálftavirkni þar sem lítil eða engin virkni er, mest áberandi í kringum 41 og 42°N. Aðrir minna áberandi staðir eru; 50.5, 49, 48.5, 44.8, 44.2 og 44°N. Svæði með aukinni virkni má sjá við 45°N. Alls fundust 27 skjálftahrinur, þær fimm stærstu allar í nálægð við þvergengi sem bendir til tengsla þar á. Gutenberg-Ricther b-gildið 1.74 var reiknað fyrir hrygginn og er nálægt því sem búist var við fyrir frárekshrygg. Skjálftavægið sýndi aukningu í átt að suðri með topp við 43°N, eftir það datt virknin niður og reis aftur í átt að suðri. Reiknuð gildi rekhraða fyrir hrygginn var 22.21-23.96 mm/ári. Stefnan byrjaði í 91.23° nyrst og endaði í 91.02° syðst á hryggnum.

Contents

x

List of Figures

List of Tables

Abbreviations

MAR: Mid-Atlantic Ridge

CGFZ: Charlie-Gibbs Fracture Zone

FPS: Focal plane solution

CGAZ: The ridge segment between the CGFZ and Azores Islands (Charlie Gibbs-Azores)

ISC: International Seismological Center

GR: The Gutenberg-Richter Law

Acknowledgements

I would like to thank my co-students that were of great assistance in numerous problems that arose during the essay. My parents provided valuable encouragement during this time and deserve thanks for that. Great thanks go out to my advisor Páll Einarsson for all the help and the many questions that arose during the writing. Lastly I would like to thank my better half for invaluable advice and encouragement. Thanks.

1 Introduction

The Mid-Atlantic Ridge marks the boundary between the North-American plate and the Eurasian plate in the north along with the N-American plate and the African plate. Further to the south the S-American Plate meets the African Plate. The ridge extends about 800 km beyond the North Pole and along the North-South axis of the Atlantic Ocean to the Bouvet Island triple junction at approximately 55°S. It is the longest mountain range found on earth stretching over 16.000 km. It was first discovered during an expedition of the HMS Challenger in 1872 led by Charles Wyville Thomson. They discovered a rise of the ocean floor while investigating a location for a transatlantic telegraph line. (Hsü, 1992). Further research revealed that the ridge extends far into the South Atlantic Ocean reaching its end near the Bouvet Island. The ridge is divided into the North- and South-Atlantic Ridge near the equator at the Romanche Trench, one of the deepest locations of the Atlantic Ocean.

The aim of this thesis is to give a an overview of the seismological activity on the Mid-Atlantic Ridge, more accurately between the Charlie-Gibbs fracture zone and the Azores. Approximately sixty years of seismological data supplied by the International Seismology Center (ISC) were examined. Seismic events, along with fault mechanism solutions will be mapped, and a frequency-magnitude distribution will be calculated. Major tectonic events such as large earthquakes and earthquake swarms will be described, along with a calculation of the total seismic moment for various ridge segments. The seafloor spreading rate will be calculated at selected location using the NUVEL 1a model and compared to previous measurements of spreading rates.

2 Regional Settings

2.1 Charlie-Gibbs Fracture Zone (CGFZ)

The CGFZ is the major fracture zone between Iceland and the Azores Islands. It offsets the ridge crest left laterally about 350 km bounded by 52° and 53°N. It was first described by Johnson (1967) and later surveyed in some detail by Fleming (1970) who showed that it is comprised of two west-east lateral valleys, separated by a ca. 45 km wide ridge. This double fracture formation is considered to be of a quite unusual nature. A median valley linking the two transform valleys at 31.5°W has produced seafloor magnetic anomalies of half spreading rate at 12.7 mm/yr. demonstrated by Searle (1981) and shown to exhibit micro seismicity by (Lilwall and Kirk, 1985; R. B. Whitmarsh, 1986). Looking at seismicity data from the International Seismological Centre on earthquakes larger than m_b 4.0, occurring from 1955 to 2015, they seem to swarm around three major sites along the CGFZ; on the northern transform valley at 35°W, the central median valley at 32°W and the southern transform valley at 30°W.

2.2 The Azores triple-junction

The Azores Islands are located at and around 38°N and 28°W, on a triple junction between the African-, North American- and Eurasian plates. The islands stretch over 600 km in relatively narrow line of 80 km along major tectonic lineaments with a WNW-ESE trend of about 116°. They are located on the so called Azores microplate which is a triangular area with active volcanism and high seismicity. A high number of tectonic lineaments are present in the area, which are responsible for most of the seismic and volcanic activity (figure 2-1). Most of the earthquakes are located on the Terceira Rift, Faial-Pico FZ, the MAR and other associated areas (Oliviera, 2004) with depths generally not exceeding 15 km. The studies of seismicity generally show shocks with normal faulting or right-lateral strike-slip along the ESE direction compatible with the eastward relative motion of the Eurasian (EU) relative to the African (AF) plate (Miranda, 1998).
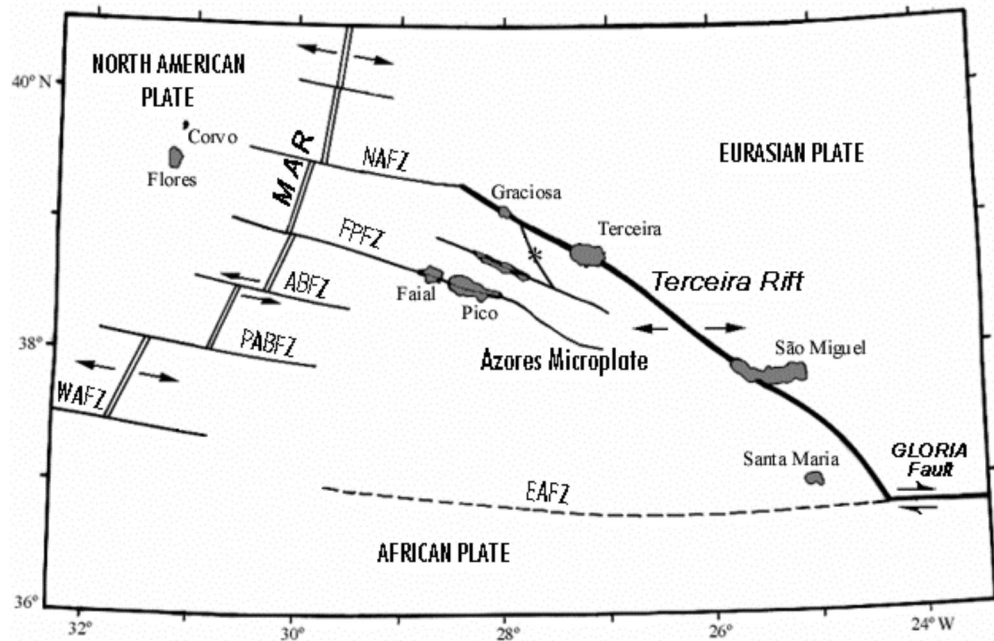
Figure 2-1: Fracture zones at the Azores triple junction. (Carlos Oliviera [from: Nunes, 1999])

2.3 **CGFZ-Azorez**

The ridge segment between the Charlie-Gibbs fracture zone and the Azores (abbreviated CGAZ in this essay) is located in the North-Atlantic Ocean with its approximate middle located 1500 km from the westernmost peninsula of Spain and follows an angular path that is more than 1450 km long. The southern part of the ridge is relatively straight and follows a trend of 014° where plate separation occurs at a right angle to the plate boundary. Earthquakes larger than magnitude 5 are rare and the frequency has been quite uniform in the past 60 years in both space and time (Einarsson, 1979). Approximately 880 km north of the Azores, the ridge changes to a trend of 341° where some interesting features have been observed. The ridge segment shows reverse faulting near 49.5°N and a second solution near 51°N shows a significant component of reverse faulting. The structure of the ridge is characterized by alternating N-S trending and oblique spreading axes. They are associated with transverse basement ridges trending slightly north of the spreading direction on both sides of the plate boundary. This so called "herringbone" pattern in the topography, interpreted by Johnson and Vogt (1973), as the result of asthenospheric flow southwards from the Iceland hot spot (Einarsson, 1986).

3

3 Fault plane solutions

Focal mechanism solutions (FMS), also referred to as fault plane solutions, are the results of an analysis of wave forms generated by earthquakes and play a major part in present day research theory of plate tectonics (Einarsson, 1987). These mechanisms provide useful information about the structure and settings of faults and can describe the crustal stress field (deformation) in which the earthquakes occur. Earthquake slip vectors on plate boundaries provide information on the relative plate motion of both sides and mechanisms of intraplate earthquakes can be used to describe possible driving mechanism of plates.

The simplest form to determine the focal mechanism of an earthquake is analyzing the first motion of P-waves. As they spread out from the epicenter, they do so in either a compressional or dilatational initial motion. A vertical seismograph records a compressional wave as an upwards motion whereas a dilatational wave is recorded as a downward motion. For optimal results, the distribution of the recording stations needs to be relatively good in relation with the earthquake epicenter. Wave motions recorded on, or near nodal planes are generally too weak to differentiate and can therefore give clues where to situate the nodal planes on the FMS (Figure 4-1). On a lower-hemisphere stereographic projection, the compressional waves are represented as a black dot and dilatational waves as an empty circle. Too weak recordings, yielding no clear motion, are represented using an X. The regions experiencing these forces are then plotted, two great circles are identified at right angles to one another that separate the dots from the circles, and that pass through or near the X symbols. These are the nodal planes, one of which coincides with the fault generated in the earthquake. (Figure 4-2) (Cronin, 2004)
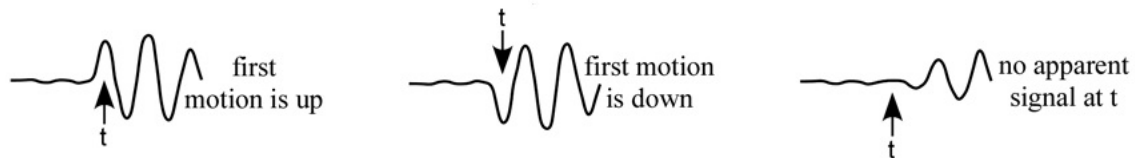
Figure 3-1: An example of seismograph recordings showing an upwards motion (compressional), a downwards motion (dilatational) and a signal too weak to discern. **(Cronin, 2004)**

Looking at figure 4-2, we see the data from a number of recording stations with the corresponding symbols plotted on diagram (a). The next diagram (b) shows where the nodal planes are identified between the tensional and compressional, using the X to situate them, resulting in a beach ball diagram (c).

However, the graphic technique as described above does not provide enough information to define the moment tensor for the earthquake. A method to do this is the double force couple, often referred to as simply *double-couple*. It brings the radiation pattern of energy emitted by an earthquake effectively into action, using a process that needs not involve a fault discontinuity. The double couple makes use of the complete waveform data and is mathematically described in 3 dimensions by a symmetrical tensor with 9 components known as the *moment tensor (M)*. It has three orthogonal axes: P (a compressive axis, of maximum shortening), T (tensional, of maximum lengthening) and N (null or B-axis). The

orientation of the axes is of interest as the fault surface along which the earthquake was generated is 45° from the P and T-axes and contains the N-axis.
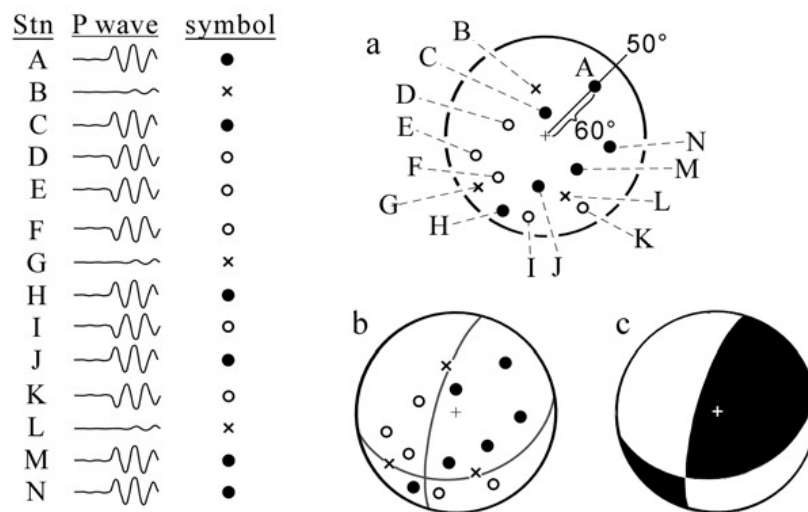
Figure 3-2: *An example of a beach ball diagram (c), and how to identify auxiliary planes using first arrivals of P-waves. The black dot represents a station recording an upwards (compressional) motion, the circle a downward (tensional) motion and the 'x' for motions too weak to differentiate.* **(Cronin, 2004)**

4 Data

The data for this project were collected using the International Seismological Center's bulletin search. (ISC, 2015). The search parameters were set to filter out earthquakes of magnitude less than 4.0 m_b from January 1955 to March 2015, defining the area of search between 39-52°N and 21-40°W. The data acquired can be seen in Appendix A. For any given event recorded the most reliable set of data was chosen and ranked using the number of stations with a preference of recording agencies where the ISC, when available, was the preferred choice.

The total count of earthquakes recorded within the parameters numbered at 1263, but due to missing or too low m_b values, the total number of events was methodically reduced to a value of 1167. The majority of the data processing was done with the application of Microsoft Excel 2010 using a QuakeML output file; an XML representation of the seismological data collected from the ISC Bulletin.

The size of an earthquake is given by its magnitude. Several different magnitude scales have been developed since C. F. Richter introduced the Richter scale (M_L) in the mid-1930s. Magnitude values discussed in this essay are: body wave magnitudes m_b, moment magnitudes M_W, and surface wave magnitudes M_S. For events with magnitudes higher than 5.5, the m_b scale starts to saturate, showing smaller values with the underestimation significantly higher with increasing size; the maximum body-wave magnitudes are around 6.5–6.8. For surface waves, a similar effect occurs, with the maximum observed values at around 8.3–8.7. The moment magnitude scale M_W is generally used for larger events, based on the seismic moment with relations to the fundamental parameters of the faulting process. Having no intrinsic upper bound, and because fault geometry and observer azimuth are a part of the computation, moment is hence a more consistent measure of earthquake size than magnitude.

All mapping was generated with the use of Esri's ArcMap software. The data for the bathymetry background was downloaded from GEBCO's website (GEBCO n.d.). Mapping was done with the aim to give as clear a picture of the seismic events occurring in the region. Interesting findings and further explanation along with the locations of the events can be seen on the various maps created to visualize the seismicity in the best way possible.

5 Discussion

5.1 Spatial distribution of epicenters

A total number of 1167 events were produced by ISC's bulletin and are shown on the overview map (*Figure 5-2*). As can be seen, the events are spread relatively uniform along the ridge segment where the larger events seem to have a slight inclination towards the bend near the middle of the ridge. Noticeable breaks in the activity on the ridge seem to occur near 49°N, 44°N, 42°N and 41°N, the most prominent located at around 42°N and 41°N. North of the bend the quakes are more spread out around the ridge axis and show slightly reduced activity compared to the southern part where the activity follows the ridge more uniformly with a seemingly higher number of events.

Quite a few intraplate events were recorded and seem to have a slight inclination towards the eastern side of the axis. For display purposes, a handful of events were excluded as they were outside the map margins.
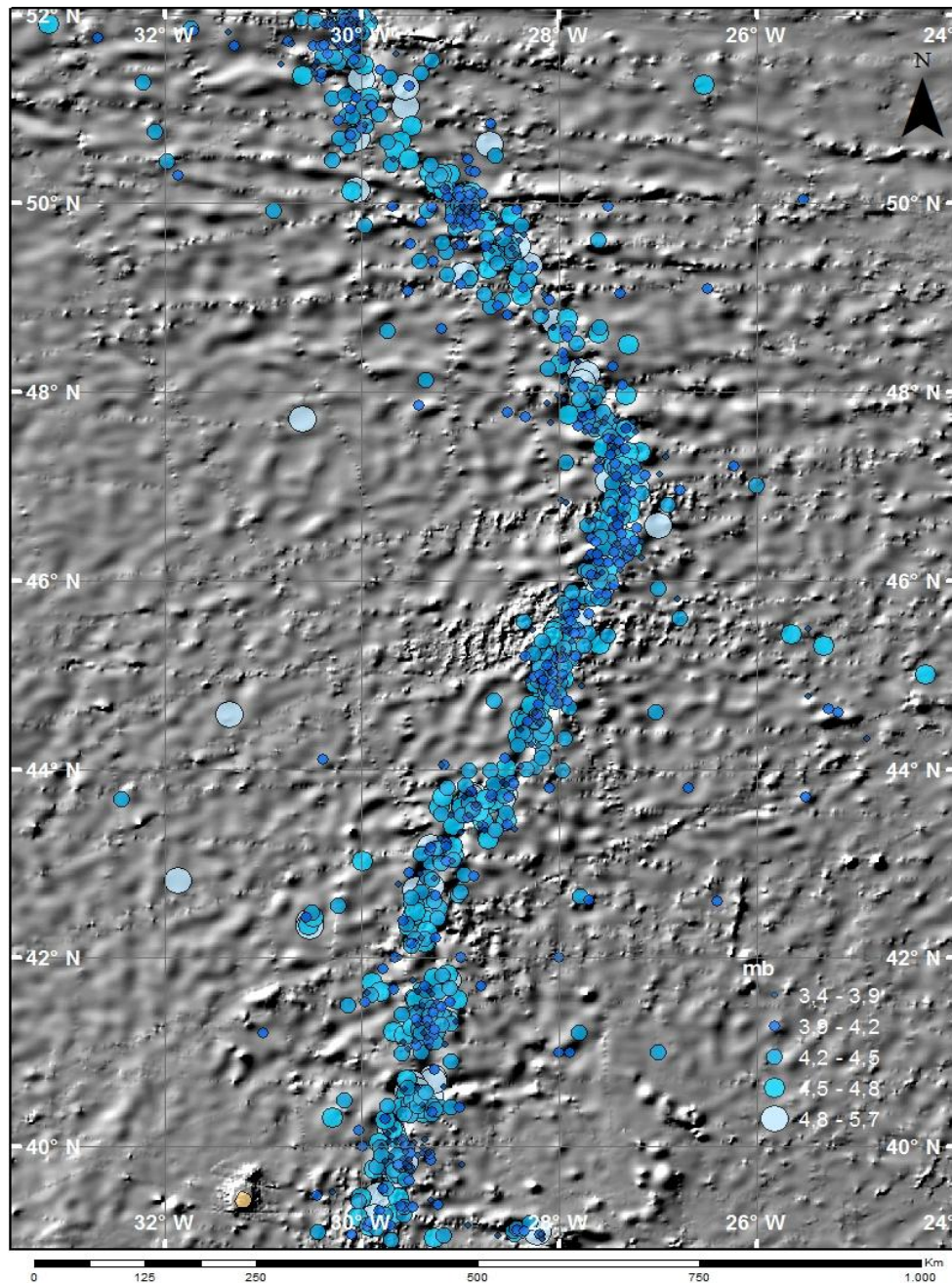
Figure 5-1: *An overview map showing epicenters for all events. Magnitude intervals were determined using Jenks natural breaks classification method integrated in the ArcMap software. Bathymetry map obtained from GEBCO. Map was made using Mercator projection.*

Notice the gap in activity in the southern part of the ridge along with the diffuse nature of the northern part in *Figure 5-1*. Larger earthquakes seem to be more dominant in the southern part of the ridge.
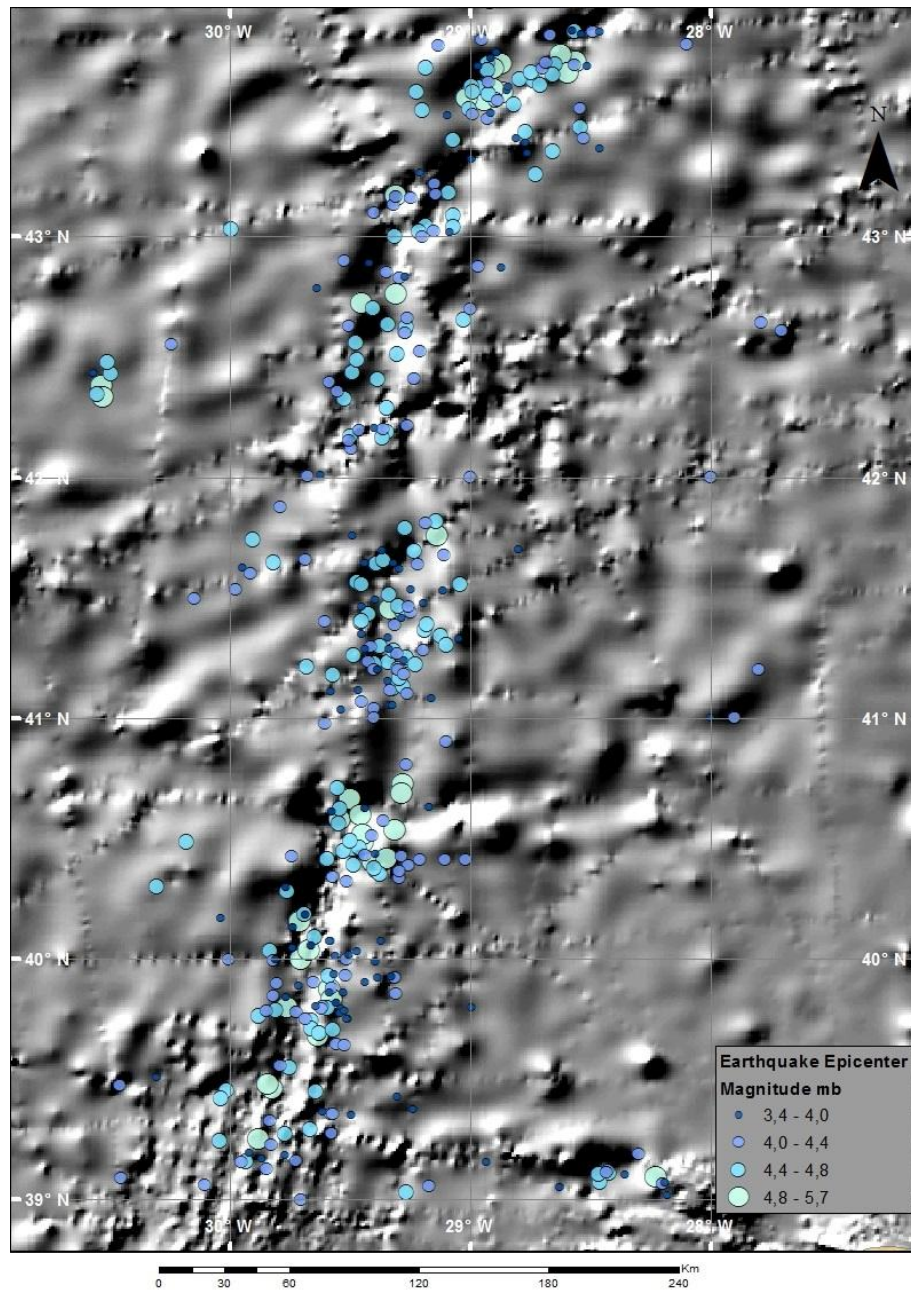
Figure 5-2: An overview of the southern part of the ridge. Notice the breaks around 42°N and 41°N. *Bathymetry map obtained from GEBCO. Map was made using Mercator projection.*

The southern part of the ridge shows some gaps in seismic activity (*Figure 5-2*), the most noticeable around 41°N and 42°N. The events are relatively well grouped and reveal areas showing increased activity.
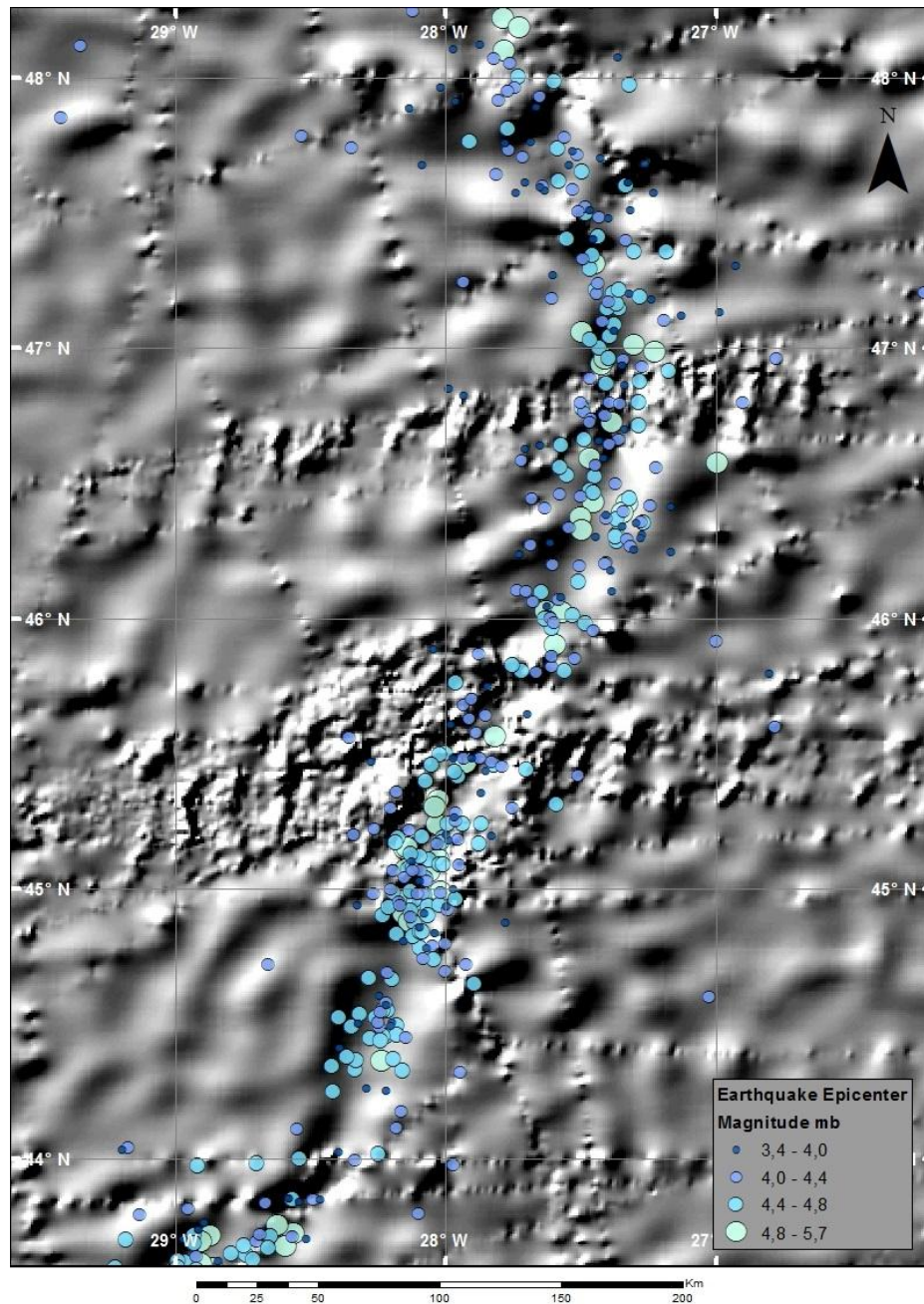
Figure 5-3: An overview of the middle part of the ridge. Bathymetry map obtained from GEBCO. Map was made using Mercator projection.

The events are quite uniform along the middle part of the ridge (*Figure 5-3*) with some signs of areas showing more concentration of events, most noticeably around 45°N. Previous studies confirm these areas of increased activity (Simao, 2010). Gaps showing little or no seismicity can be seen on the southern part of the segment, around 44.2 and 44.8°N.
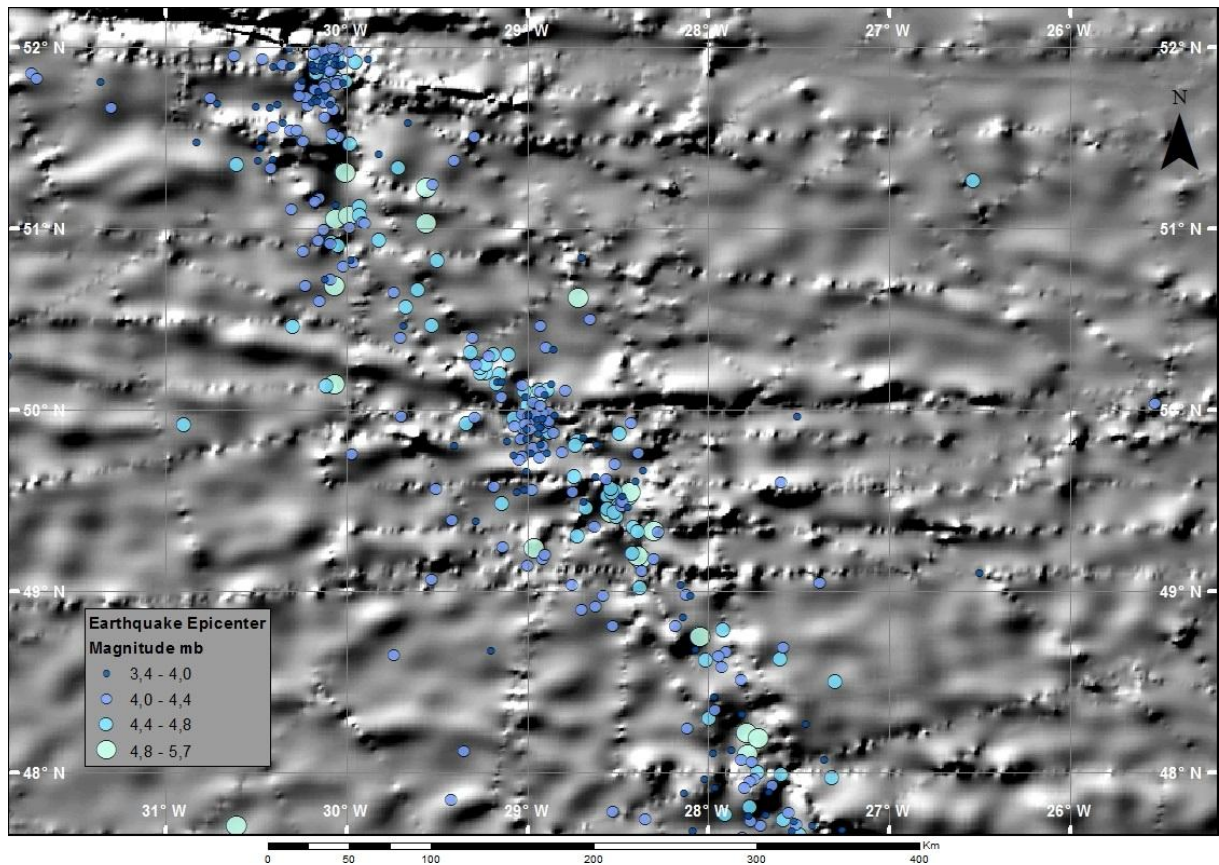
Figure 5-4: An overview of the northern part of the ridge. Bathymetry map obtained from GEBCO. Map was made using Mercator projection. Notice how the events are spread around the axis in contrast to the middle and southern parts of the ridge.

In Figure 5-4 you see the more spread out nature of the event distribution. A number of faults are located on this part of the ridge. Of the few reverse faulting observed, two of them occurred on this part of the ridge (*Figure 5-5*). A third event showing reverse intraplate faulting can be seen on the lower left margin of the map marked with a light blue dot.

Two places on this ridge segment show a higher concentration of events, around 51.8°N and 50°N, the rest showing no clear trend of event distribution.
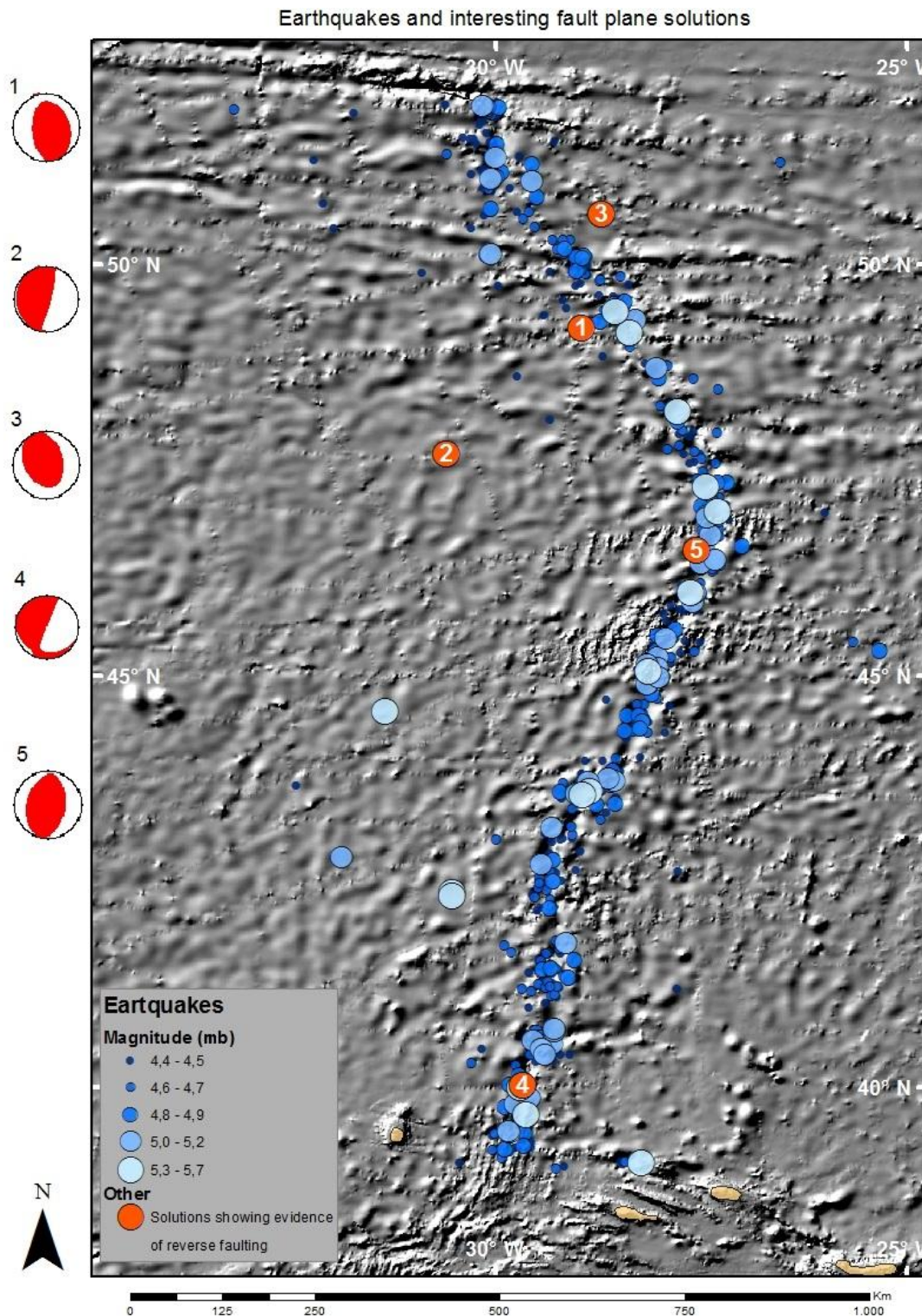
Figure 5-5: *An overview of events showing locations of reverse faulting. Bathymetry map obtained from GEBCO. Map was made using Mercator projection.*

Out of the five events showing significant component of reverse faulting (*Figure 5-5*) four of them occurred on the ridge with one intraplate event to the west of the ridge. Looking at the size of the earthquakes, a slight trend of larger magnitudes towards the bend in the ridge, as previously mentioned, can be seen.

13
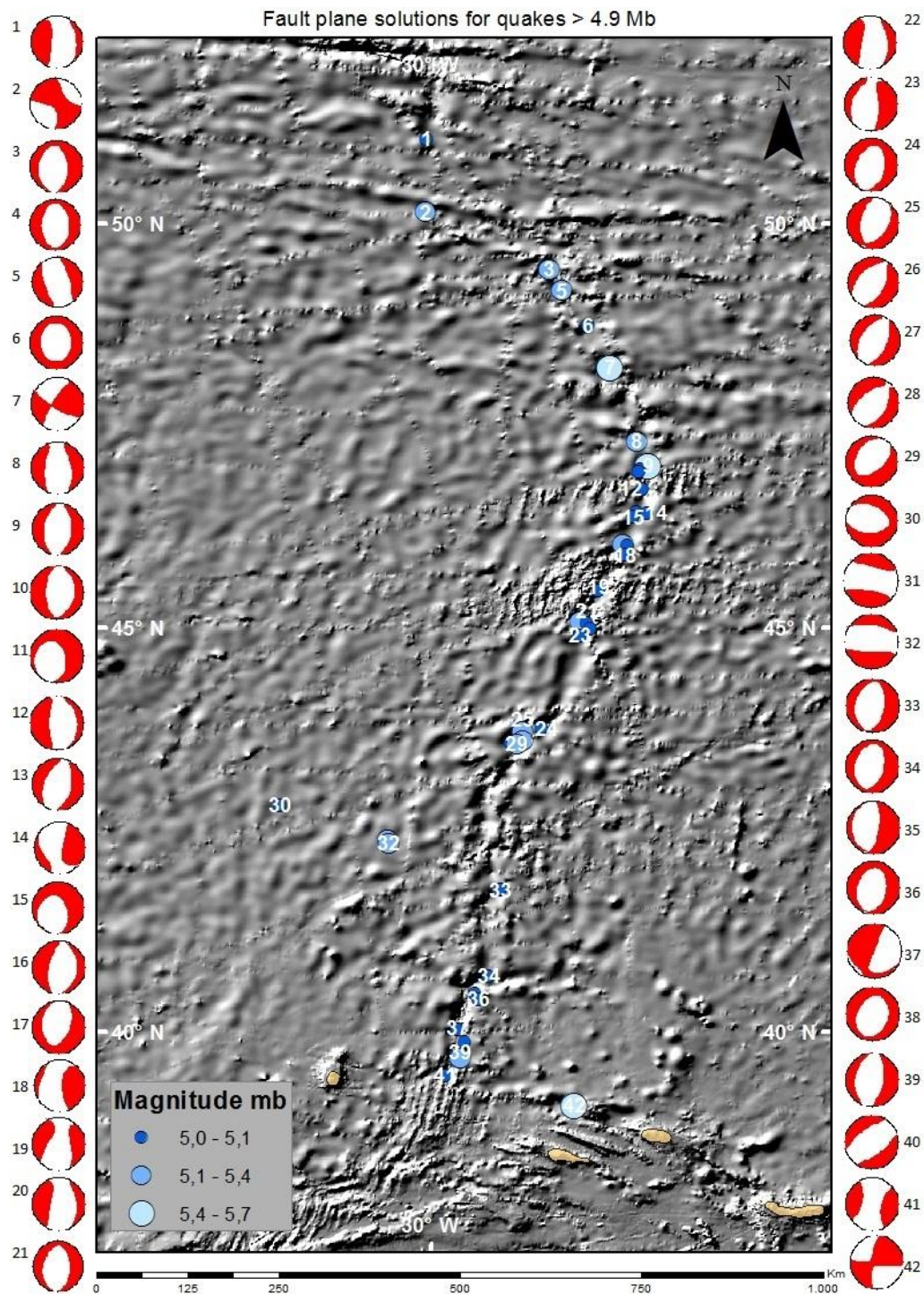
Figure 5-6: *An overview map showing locations of fault plane solutions recorded by the International Seismological Center. Bathymetry map obtained from GEBCO. Map was made using Mercator projection.*

As seen in *Figure 5-6*, a number of fault mechanism solutions were produced during the period from 1955-2015. Of the FMS's, most show evidence of normal faulting with a few strike-slip events that seem to coincide with faults on the ridge. Reverse faulting can't be seen in the larger events with the exception of solution 37 showing signs of reverse faulting with a strike-slip element. The solutions show a trend close to the axis with two exceptions, 30 and 32, both have elements of normal faulting, the former showing a higher percentage of double-couple.

5.2 Large seismic events

A fair number of large earthquakes were observed on the ridge segment between 1955 and 2015. Of the 1167 seismic events recorded, 76 had an m_b value of 5.3 or higher, 8 of which produced a moment magnitude M_W (*Table 5-1*). Two events share the first place with a moment magnitude of 5.9; however, they differ in m_b readings where one measures at 5.6 and the other 5.5. The one showing the higher value took place in June 1989 approximately 14 km WNW of Graciosa, the northernmost island in the central group of the Azores, while it's facsimile occurred in December 2008 south of the Maxwell FZ on MAR. Both events produced a focal mechanism with the '89 event showing signs of strike-slip faulting with a high double-couple component. The 2008 event produced a solution indicating a normal fault dip-slip mechanism.

Table 5-1: *Largest single events that occurred during the time period from 1955-2015. Focal mechanism solutions from the International Seismological Center.*

Event ID	Mw	mb	Location		Date	Focal Mechanism
402983	5,9	5,6	39.10°N	28.23°W	26/06/1989	
13813945	5,9	5,5	47.01°N	27.30°W	19/12/2008	
3036443	5,6	5,7	48.22°N	27.79°W	17/05/2002	
17103712	5,6	5,3	43.60°N	28.86°W	31/08/2011	
603503054	5,5	5,4	49.44°N	28.54°W	30/09/2013	
7215688	5,5	5,3	39.68°N	29.63°W	23/12/2003	
13229608	5,5	5,3	42.38°N	30.53°W	24/05/2008	
14192631	5,5	5,3	42.30°N	30.53°W	17/12/2009	

The largest intraplate earthquake recorded in the region occurred in 1972 approximately 750 km west in the northern part of the ridge.

5.3 Earthquake sequences and swarms

An earthquake sequence is a group of earthquakes that occur closely in both space and time and includes a mainshock that is noticeably larger than the following aftershocks. Where a distinct mainshock is not present however, the procession is referred to as a swarm. Mainshocks were decidedly absent in the data for this area. In this essay, a sequence is defined as a series of no less than five earthquakes, taking place in close proximity in both time and space.

Table 5-2: *Largest earthquake sequences that occurred during the time period from 1955-2015. The sequences are listed in the order of size (count)*

First event	Last event	Location		Count	Largest (mb)	FMS
14/03/1996	1/04/1996	51.05°N	30.06°W	68	5.0	
28/09/2009	13/10/2009	46.43°N	27.33°W	28	5.1	
20/01/1968	22/01/1968	41.18°N	29.57°W	22	4.7	N/A
17/06/2012	27/06/2012	41.76°N	29.14°W	18	5.0	
10/10/1989	14/10/1989	50.03°N	29.00°W	17	4.7	N/A

No earthquake sequences with distinct main shocks were found in the data that matched the criteria previously mentioned. A total number of 27 sequences took place during the 60 year period with information on the five largest occupying *Table 5-2*. The largest and the smallest took place on the southern part with the second largest near the middle of the ridge. The sequences recorded occur relatively uniform along the ridge with the exception between 46.7-48.1°N where no sequenced events were recorded.
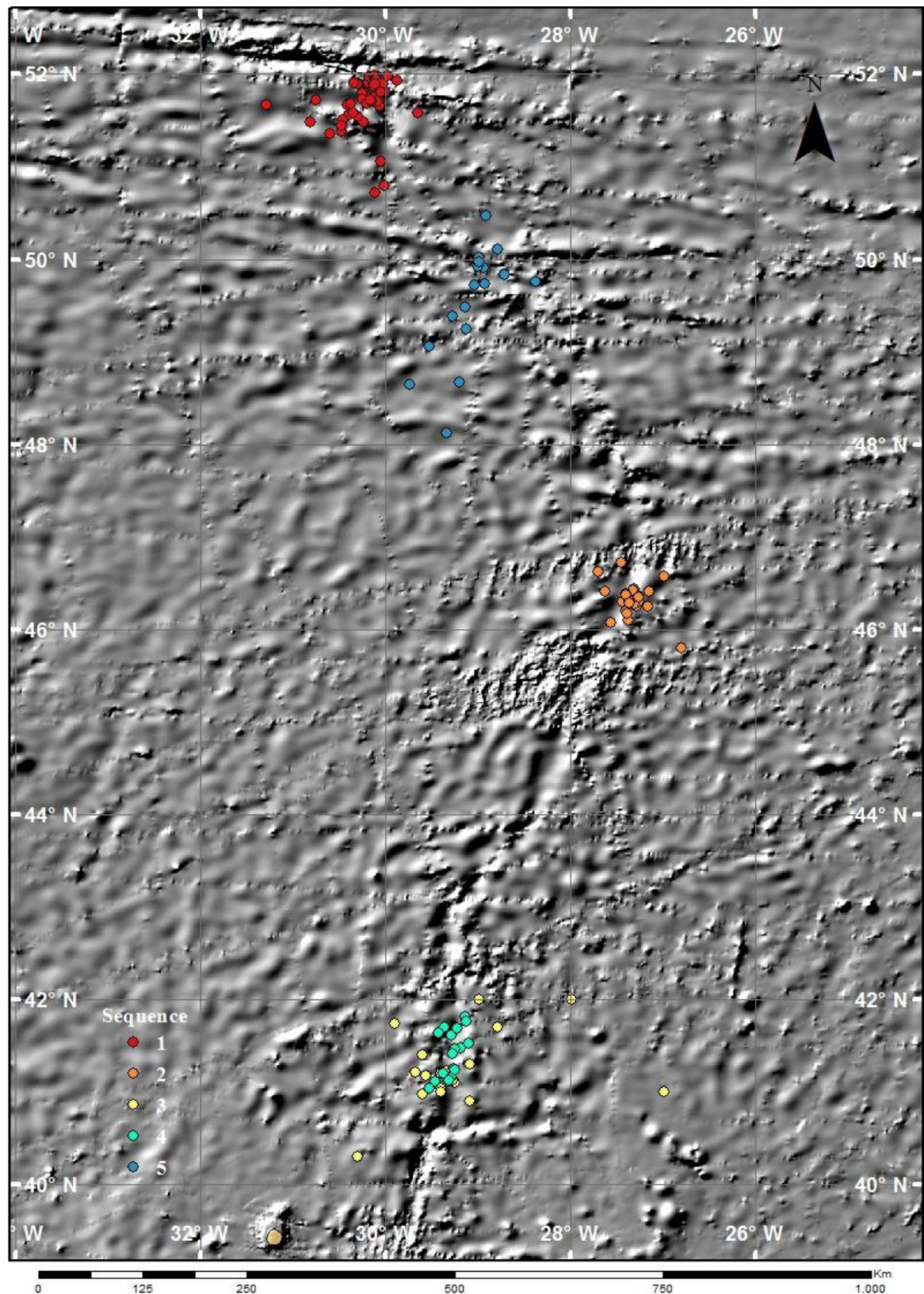
Figure 5-7: An overview map showing the five largest earthquake sequences, No. 1 being the largest. *Bathymetry map obtained from GEBCO. Map was made using Mercator projection.*

5.4 **Seismic Moment**

The seismic moment (M_0) is a quantity that defines the size of an earthquake. It is based on three parameters: the area of rupture (**F**) along the fault, the shear modulus of the material involved in the earthquake (**μ**), the average displacement (**u**) of the area of rupture. The relation of M_0 and M_w is shown in the following equation (Fowler, 1990):

$$M_w = \frac{2}{3} log_{10}(M_0) - 6.0 \qquad \qquad (5\text{-}1)$$

A little over an eighth (12,86%) of the seismic data yielded an M_w value. The m_b value will be used for calculations as the correlation between the two is relatively good. Using the Microsoft Excel correlation coefficient calculation it yields a value of 0,741008.
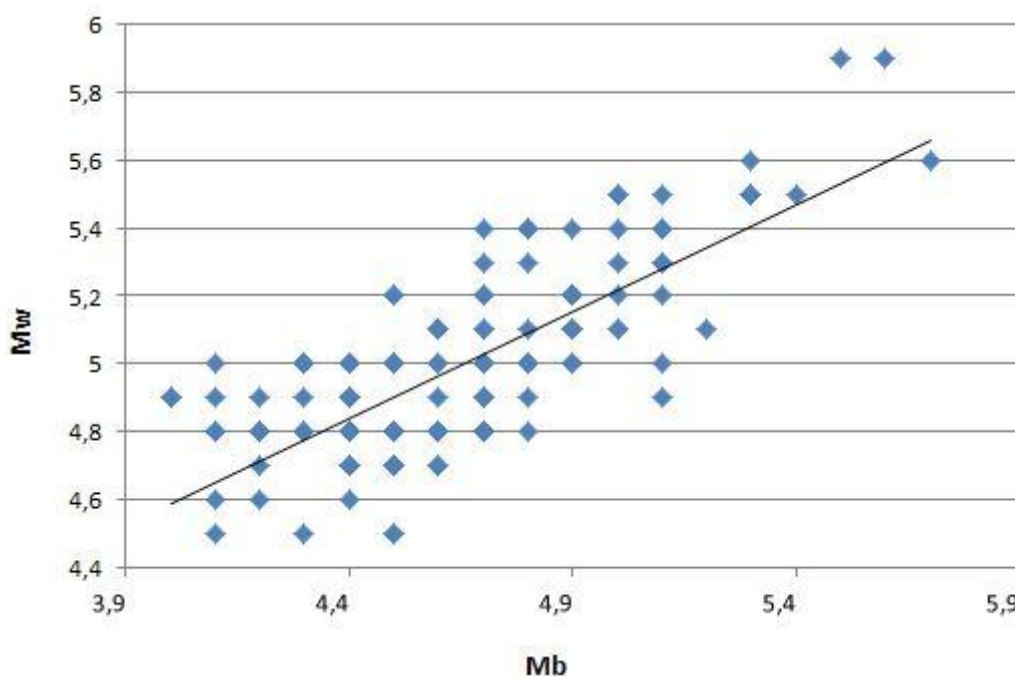
Figure 5-8: $m_b \geq 4.0$ *as a function of M_w. Correlation is 0,741008. Calculations and graph were produced using Excel.*

The ridge was divided into segments in order to calculate the seismic moment and instead of the M_w, the m_b value is used in equation (5-1). Calculations for M_0 were performed for all single events on the ridge with the exception of intraplate earthquakes that were offset by more than a rough estimate of 100 km from the ridge axis. Filtration was done manually due to the curvature of the ridge and may vary slightly as a result. To simplify the calculations and give a good overview, the ridge was split into 26 equal segments, the length being 1° latitude. See *Figure 5-9*. Looking at the moment peaks, they show an increase as we move southward along the ridge with a noticeably abrupt decrease as we get to 43°N, rising again towards the Azores.
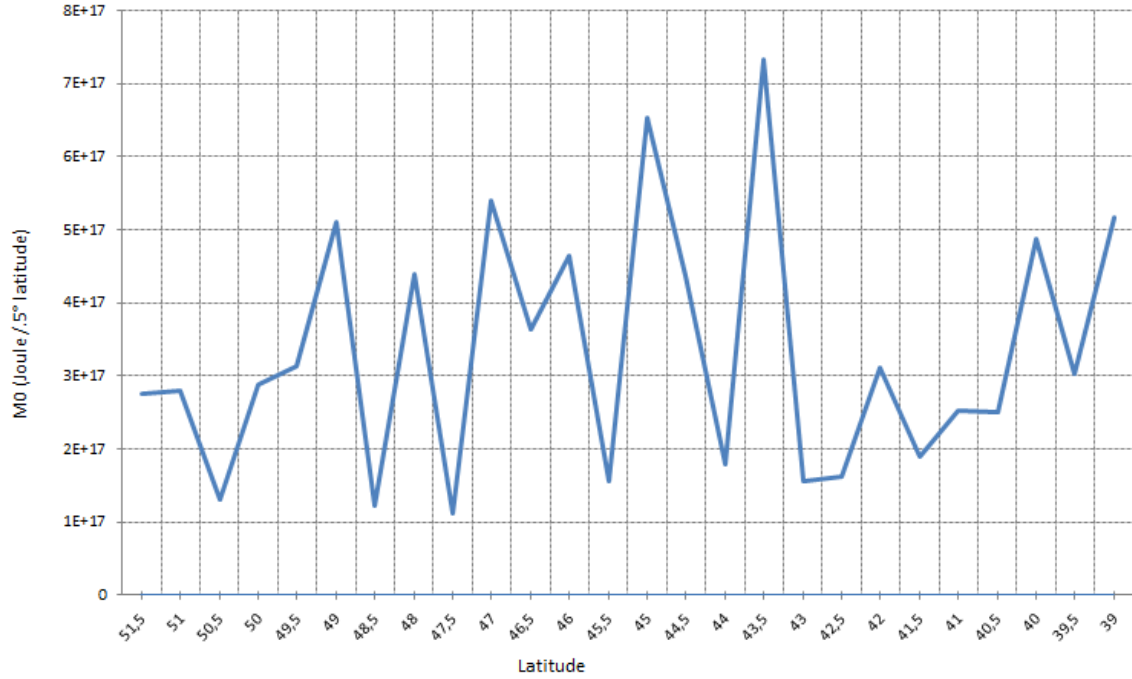
Figure 5-9: *Seismic moment (M$_0$) distribution along the MAR ridge divided into segments of half a degree latitude. The bottom axis displays the lower mark of each segment.*

Of the peaks observed, one included an event showing strong evidence of strike-slip faulting (48°N), one with evidence of reverse faulting (49°N), where others all showed signs of normal faulting. Looking at the data and projections, a larger number of events with a higher magnitude value coincide with peaks in the graph. The largest peak located around 43.5°N reveals a drop of lower magnitude values with a higher percentage of larger events in the defined segment of the ridge. The same applies for the second largest peak at 45°N.

Table 5-3: *Moment magnitude results divided into segments of .5° latitude.*

Latitude	M$_0$	Latitude	M$_0$
51,5	2,75E+17	45	6,53E+17
51	2,79E+17	44,5	4,38E+17
50,5	1,3E+17	44	1,8E+17
50	2,87E+17	43,5	7,32E+17
49,5	3,12E+17	43	1,55E+17
49	5,09E+17	42,5	1,61E+17
48,5	1,22E+17	42	3,11E+17
48	4,39E+17	41,5	1,89E+17
47,5	1,13E+17	41	2,51E+17
47	5,4E+17	40,5	2,49E+17
46,5	3,64E+17	40	4,87E+17
46	4,64E+17	39,5	3,02E+17
45,5	1,56E+17	39	5,17E+17

5.5 **Gutenberg-Richter Relationship**

Charles Francis Richter and Beno Gutenberg published a paper in 1956 about the relationship between earthquake magnitude and frequency. It states that the distribution of earthquakes in a given location on the earth typically in accord with the Gutenberg-Richter Law (GR):

$$Log_{10}(N) = A - bM \qquad (5\text{-}2)$$

GR is a power law and approximately linear. N is the cumulative number of quakes larger then magnitude M whereas a and b are scaling parameters, a describing the amount of total seismicity, b describing the frequency of small earthquakes where a higher value indicates a larger proportion of smaller earthquakes. Take a number of events greater than any magnitude, apply logarithm and it will be proportional to magnitude. In short, given a magnitude 5.0, there will be 10 times the amount of earthquakes of magnitude 4.0, a 100 times more of magnitude 3.0 etc (Crampin & Gao, 2015).

In this essay the *maximum likelihood estimation* will be used along with an estimation of error, formulas are as following:

$$b = \frac{4{,}3}{M_{avg} - M_{min}} \qquad (5\text{-}3)$$

$$e = \frac{b}{\sqrt{n}} \qquad (5\text{-}4)$$

In a frequency-magnitude distribution graph, the negative of the slope is equal to the b-value. M_{avg} is determined by finding the average of all earthquakes with magnitudes $M \geq M_{min}$. The sensitivity of the seismograph system or network is determined by finding the point where the graph line goes banana. That is to say, where the line starts to bend and roll off the linear slope. This point indicates the M_{min} value. At this point, the system of seismographs have picked up about all there is to be detected of that magnitude and higher. It is likely that this value has gradually been lowering as seismograph networks increase their sensitivity by adding station locations and/or improving technology (C. Godano, 2014).
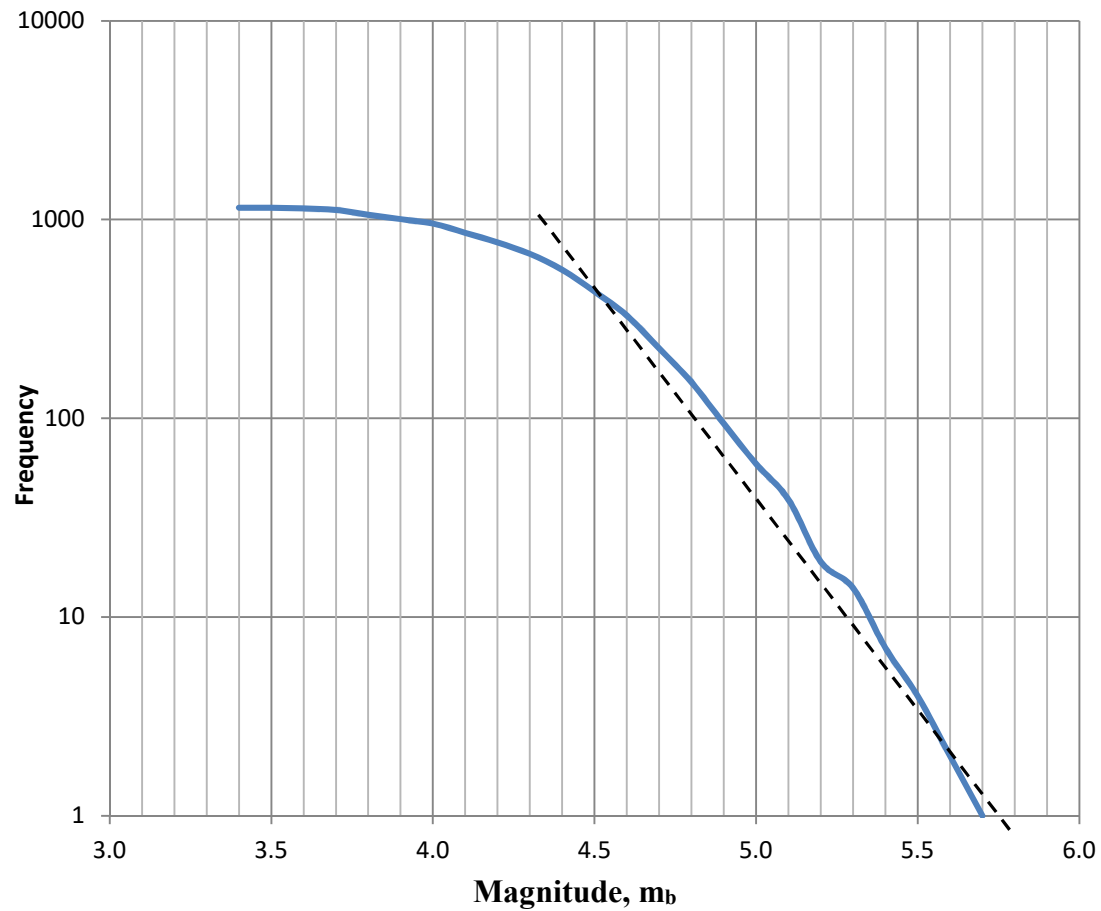
Figure 5-10: *A frequency-magnitude plot for the ridge events.*

In *Figure 5-10* we see a frequency-magnitude plot for events recorded on the ridge. A plot was done for both m_b and M_s magnitudes, leaving out the latter due to a low number of events recorded for that magnitude. The slope, as can be seen, is relatively linear with a slight curve. This curve makes it a little more difficult to determine where the "knee" or roll-off value M_{min} resides. It seems to be located at or around magnitudes 4.5 to 4.7 with 4.6 being the likeliest candidate.

Table 5-4: *Gutenberg-Richter calculation results.*

M$_{min}$	M$_{avg}$	b	err	A
4.6	4.65	1.74	0.096	10.52

The results above in *Table 5-4* produced using the aforementioned M$_{min}$ value of 4.6 m$_b$.

5.6 **Spreading Rate**

A spreading rate indicates how fast two tectonic plates are moving away from one another on a divergent plate boundary. Methods to calculate the rate of movement are an important factor of studying spreading ridges and several methods exist. According to the NUVEL-1A model, the pole of relative rotation for the North-American and Eurasian plates is situated in North Siberia at 62.4°N, 135.8°E with an angular velocity of 0.22°/Ma.

In the first step to calculate the plate motion, we need to find the magnitude and azimuth of the velocity vector. The following formulas are used to that end:

$$v = \omega R sin a \tag{5-5}$$

$$\beta = 90° + C \tag{5-6}$$

Table 5-5: *Variables and constants used for calculating plate velocity*

λ_p	Latitude of rotation pole
ϕ_p	Longitude of rotation pole
λ_x	Latitude of point on plate boundary
ϕ_x	Longitude of point on plate boundary
v	Velocity on plate boundary
β	Azimuth of velocity on plate boundary
R	Radius of Earth
ω	Angular velocity about rotation pole

With the radius of Earth known at 6380 km along with the angular velocity ω = 0.22°/*Ma*, we use trigonometry and acquire the following formulas:

$$a = cos^{-1}(sin(\lambda_x) sin(\lambda_p) + cos(\lambda_x) cos(\lambda_p) cos(\phi_p - \phi_x) \tag{5-7}$$

$$C = sin^{-1} \left(\frac{cos(\lambda_p) sin(\phi_p - \phi_x)}{sin(a)} \right) \tag{5-8}$$

Calculations were done for the ridge on several locations with .5° latitude intervals. See *Table 5-6* for the results.

Table 5-6: *Calculations of amplitude and direction for relative plate motion*

Latitude (°)	Longitude (°)	Rek (mm/yr)	Azimuth (°)
52.0	-30.00	22.21	91.02
51.5	-29.93	22.30	91.03
51.0	-29.88	22.39	91.03
50.5	-29.46	22.46	91.04
50.0	-28.88	22.54	91.05
49.5	-28.42	22.62	91.05
49.0	-28.10	22.69	91.06
48.5	-27.65	22.76	91.07
48.0	-27.53	22.84	91.07
47.5	-27.39	22.91	91.08
47.0	-27.28	22.99	91.09
46.5	-27.39	23.06	91.09
46.0	-27.53	23.13	91.10
45.5	-27.79	23.20	91.10
45.0	-28.01	23.27	91.11
44.5	-28.17	23.34	91.12
44.0	-28.39	23.41	91.13
43.5	-28.81	23.47	91.13
43.0	-29.10	23.54	91.14
42.5	-29.24	23.60	91.15
42.0	-29.05	23.65	91.16
41.5	-29.15	23.71	91.17
41.0	-29.12	23.76	91.18
40.5	-29.29	23.81	91.20
40.0	-29.44	23.86	91.21
39.5	-29.50	23.91	91.22
39.0	-29.91	23.96	91.23

The velocity increases as we move south along the ridge. Starting with 22.21 mm/yr closest to the CGFZ and ending in 23.96 at the Azores. These findings are in unison with previous findings in the area (Searle, 1986)

6 Conclusions

1) The northern part of the ridge has a slightly more diffuse nature than of events south of the bend in the ridge. The frequency and compactness are also slightly higher to the south.

2) Areas showing little or no activity were observed on several sites on the ridge. The most prominent located around 42°N and 41°N. The reason for the gaps is currently unknown. Other locations are 50.5°N, 49°N, 48.5°N, 44°N, 44.8°N and 44.2°N.

3) The fault plane solutions on the ridge mostly show normal faulting which is to be expected on a spreading ridge. A few quakes showed reverse or transform faulting coinciding with transforms on the ridge.

4) 76 Earthquakes had an m_b value of 5.3 or higher, 8 of which produced a moment magnitude M_W. Of the 8 largest earthquakes, 3 occurred on the northern part of the ridge, evenly spread along the ridge, approximately 150 km apart with one event showing strike-slip faulting. 2 took place approximately 9 km apart, around 120 km west of the ridge. The last two occurred close to the Azores, one a few km NNW of the island of Graciosa, the other on the southernmost part of the ridge near the Azores transforms. Of the events mentioned above, the quakes occurring on the ridge all originated in a close proximity to transform faults.

5) 27 swarms were recorded during the time period. The five largest all had close proximity to transform faults. A link between the two is a likely possibility.

6) The Gutenberg-Richter b-value of 1.74 for the ridge is close to expected values for mid-ocean ridges.

7) The seismic moment shows an increasing trend towards the south, peaking at 43-43.5°N with a noticeable drop and increasing again towards the Azores.

8) Spreading rates and azimuth calculated for the ridge are in unison with previous studies ranging from 22.21-23.96 mm/yr. and the azimuth from 91.23° to 91.02° (north-south).

9) Intraplate earthquakes are relatively common and mostly showing thrust faulting when available, which is common except in close proximity to spreading ridges.

10) The ridge section shows behavior similar to that of a typical mid-ocean spreading ridge. Seismic moment shows an increase towards the south, dropping suddenly around 43°N and with a continuing increase towards the Azores. Near all fault plane solutions agree with spreading ridge behavior with some anomalies most likely explained by transforms on the ridge.

7 Works Cited

Godano, C., Lippiello, E. and de Arcangelis, L., 2014. Variability of the b value in the Gutenberg–Richter distribution. *Geophysical Journal International*, *199*(3), pp.1765-1771.

Crampin, S. and Gao, Y., 2015. The physics underlying Gutenberg-Richter in the earth and in the moon. *Journal of Earth Science*, *26*(1), pp.134-139.

Cronin, V., 2004. A primer on focal mechanism solutions for geologists. A full-text pdf available from the author, Vince_Cronin@baylor.edu

Einarsson, P., 1979. Seismicity and earthquake focal mechanisms along the Mid-Atlantic plate boundary between Iceland and the Azores.*Tectonophysics*, *55*(1-2), pp.127-153.

Einarsson, P., 1986. Seismicity along the eastern margin of the North American Plate. in Vogt, P.R., and Tucholke, B.E., eds., The Geology of North America, Vol. M, The Western North Atlantic Region: Geological Society of America, p. 99-116

Einarsson, P., 1987. Compilation of earthquake fault plane solutions in the North Atlantic and Arctic Oceans. In: Recent Plate Movements and Deformation, ed. K. Kasahara, Geodynamics Series, Vol. 20, Am. Geophys. Union, p. 47-62

Fowler, C.M.R., 1990. *The solid earth: an introduction to global geophysics*. Cambridge University Press.

GEBCO. (n.d.). *Gridded Bathymtry data [Web Page]*. Retrieved from: http://www.gebco.net/data_and_products/gridded_bathymetry_data/

Hsü, Kenneth Jinghwa. *Challenger at sea: a ship that revolutionized earth science*. Princeton University Press, 2014.

ISC. (2015). *ISC Bulletin [Web Page]*. Retrieved from International Seismological Centre: http://isc-mirror.iris.washington.edu/iscbulletin/search/bulletin/

Miranda, J.M., Victor, L.M., Simões, J.Z., Luis, J.F., Matias, L., Shimamura, H., Shiobara, H., Nemoto, H., Mochizuki, H., Hirn, A. and Lépine, J.C., 1998. Tectonic setting of the Azores Plateau deduced from a OBS survey. *Marine Geophysical Researches*, *20*(3), pp.171-182.

Olaiz, A.J., Muñoz-Martín, A., De Vicente, G., Vegas, R. and Cloetingh, S., 2009. European continuous active tectonic strain–stress map.*Tectonophysics*, *474*(1), pp.33-40.

Oliveira, C.S., Sigbjörnsson, R. and Ólafsson, S., 2004, August. A comparative study on strong ground motion in two volcanic environments: Azores and Iceland. In *Proceedings of the 13th World Conference on Earthquake Engineering* (p. 13).

Whitmarsh, R.B. and Calvert, A.J., 1986. Crustal structure of Atlantic fracture zones—I. The Charlie-Gibbs fracture zone. *Geophysical Journal International*, *85*(1), pp.107-138.

Searle, R.C., 1986. GLORIA investigations of oceanic fracture zones: comparative study of the transform fault zone. *Journal of the Geological Society*, *143*(5), pp.743-756.

Simao, N., Escartin, J., Goslin, J., Haxel, J., Cannat, M. and Dziak, R., 2010. Regional seismicity of the Mid-Atlantic Ridge: observations from autonomous hydrophone arrays. *Geophysical Journal International*, *183*(3), pp.1559-1578.

Sykes, L.R., 1967. Mechanism of earthquakes and nature of faulting on the mid-oceanic ridges. *Journal of Geophysical Research*, *72*(8), pp.2131-2153.

Appendix A

EventID	Date	Latitude	Longitude	mb	Mw	Strike/Dip/Rake	P Az/Pl	T Az/Pl	N Az/Pl	Author
402983	26.06.89	39.0951	-28.2271	5,6	5,9	105/32/-110	248/72	29/14	122/11	HRVD
6144040	30.11.02	39.1102	-28.4207	4,7	5,2	106/45/-129	300/63	42/6	135/27	HRVD
2430830	07.11.01	39.128	-29.847	4,3	5,0	161/65/-93	64/70	253/19	162/3	ZUR_RMT
14703083	14.05.10	39.2872	-29.6629	4,8	5,0	24/39/-78	56/80	285/7	194/8	GCMT
603171902	01.07.13	39.448	-29.638	4,8	4,8	34/61/-84	318/73	119/16	211/5	GCMT
601838165	18.10.12	39.4508	-30.0116	4,6	4,9	79/66/-67	25/62	152/18	249/21	GCMT
329899	23.06.91	39.4627	-29.8232	5,1		147/90/-180	12/0	102/0	180/90	HRVD
393201	23.09.89	39.4799	-29.839	5,1		53/45/-90	180/90	143/0	53/0	HRVD
12807835	18.08.07	39.5553	-29.789	4,1	5,0	2/26/-121	149/65	295/21	30/13	GCMT
7401571	15.09.04	39.6466	-29.5553	4,3	4,8	2/22/-90	91/67	272/23	182/0	ZUR_RMT
7215688	23.12.03	39.6783	-29.6324	5,3	5,5	27/36/-65	46/71	279/11	186/15	HRVD
7401585	15.09.04	39.7033	-29.57	4,5	5,2	10/45/-72	6/78	268/2	178/12	ZUR_RMT
3483838	19.07.02	39.793	-29.618	4,1	4,8	18/70/-84	297/65	103/25	196/5	ZUR_RMT
432110	22.07.88	39.8747	-29.5851	5,0		11/42/-103	178/81	290/3	21/8	HRVD
6531288	05.01.03	39.8801	-29.5737	4,3	5,0	176/62/-89	88/73	265/17	355/1	ZUR_RMT
8860271	05.11.06	39.926	-29.5881	4,6	4,8	1/49/-96	228/84	95/4	4/4	GCMT
7183425	14.11.03	40.0376	-29.6708	5,1	5,0	111/22/-1	91/41	312/41	202/22	HRVD
603346988	24.08.13	40.1704	-30.0366	4,0	4,9	27/21/-127	174/59	326/28	62/12	GCMT
604373872	30.03.14	40.1827	-29.6834	3,9	4,8	1/34/-137	181/59	304/18	43/24	GCMT
603441589	18.09.13	40.2766	-29.7601	4,6	4,7	28/58/-87	306/77	116/13	207/2	GCMT
10623578	23.02.08	40.3654	-29.3916	4,8	4,9	215/30/-52	232/63	98/19	2/18	GCMT
13214710	23.02.08	40.4037	-29.4041	5,1	5,3	6/48/-101	211/81	103/3	13/8	GCMT
1738492	31.07.00	40.412	-29.591	4,6	4,8	19/74/-87	292/61	107/29	198/2	ZUR_RMT
2437016	26.12.01	40.416	-29.346	4,9	5,0	157/22/-75	222/65	56/24	323/5	HRVD
2437018	26.12.01	40.428	-29.282	4,4	4,9	21/39/-83	67/83	286/6	195/5	ZUR_RMT
1738490	31.07.00	40.444	-29.526	4,5	4,7	36/14/-80	112/58	298/31	206/2	ZUR_RMT
1738496	31.07.00	40.461	-29.461	4,7	4,8	18/23/-87	103/68	286/22	196/1	ZUR_RMT
1738494	31.07.00	40.482	-29.445	5,1	5,4	8/70/-86	285/65	95/25	187/4	HRVD
1738500	31.07.00	40.488	-29.498	4,5	4,7	2/74/-91	271/61	92/29	2/1	ZUR_RMT
1738498	31.07.00	40.518	-29.445	4,9	5,2	213/45/-22	187/44	79/18	333/41	HRVD
13214714	23.02.08	40.6875	-29.2851	5,0	5,1	13/52/-92	271/82	105/7	14/2	GCMT
10397049	28.01.07	41.0547	-29.3211	3,8	4,8	209/50/-60	185/68	278/1	9/22	GCMT
601192730	24.06.12	41.1145	-29.3309	4,2	4,8	8/25/-107	131/68	291/20	23/7	GCMT
601195979	25.06.12	41.1202	-29.3227	4,6	5,1	4/41/-98	151/83	280/4	11/5	GCMT
601192732	24.06.12	41.1642	-29.2916	4,5	5,0	13/44/-98	186/85	288/1	18/5	GCMT
7374298	21.07.04	41.1809	-29.275	4,2	4,8	54/63/-69	2/65	129/15	224/19	ZUR_RMT
1763805	31.01.01	41.22	-29.227	4,5	5,0	8/81/-92	275/54	100/36	8/2	ZUR_RMT
601197139	27.06.12	41.239	-29.2586	4,7	4,8	2/38/-102	146/80	281/7	12/7	GCMT
1912500	21.10.00	41.284	-29.194	4,3	5,0	31/76/-94	296/59	124/31	32/4	ZUR_RMT
1763807	31.01.01	41.299	-29.373	4,7	5,4	23/61/-89	296/74	113/16	203/1	ZUR_RMT
7472009	14.02.05	41.3869	-29.1802	4,5	4,8	8/25/-79	76/70	270/20	178/5	ZUR_RMT
7451055	23.12.04	41.4387	-29.2458	4,4	4,7	46/46/-64	35/71	298/2	207/18	ZUR_RMT
126042	22.01.95	41.4551	-29.3324	4,9		11/58/-93	270/77	103/13	12/3	HRVD
601468005	17.06.12	41.4644	-29.2553	4,2	4,9	32/51/-74	1/77	111/5	202/12	GCMT
601126699	17.06.12	41.4789	-29.1912	4,0	4,9	7/30/-54	27/64	251/19	155/17	GCMT
1808824	19.06.00	41.64	-29.215	4,4	4,6	15/37/-79	56/79	276/8	185/7	ZUR_RMT
3322105	12.06.01	41.655	-29.359	4,5	4,8	8/65/-87	285/69	95/20	186/3	ZUR_RMT
601126723	18.06.12	41.6908	-29.232	4,6	4,8	203/45/-50	190/62	86/7	353/27	GCMT
601125928	18.06.12	41.7589	-29.1363	5,0	5,1	9/52/-93	263/82	101/7	11/2	GCMT
1755710	31.08.00	41.809	-29.182	4,4	4,9	20/75/-90	291/60	110/30	200/0	ZUR_RMT

EventID	Date	Latitude	Longitude	mb	Mw	Strike/Dip/Rake	P Az/Pl	T Az/Pl	N Az/Pl	Author
14192631	17.12.09	42.3344	-30.5265	5,3	5,5	77/49/-117	277/70	186/0	96/20	GCMT
13229608	24.05.08	42.3822	-30.5307	5,3	5,5	75/56/-128	287/59	191/4	98/31	GCMT
11528551	05.01.09	42.4316	-30.4939	4,6	5,1	76/62/-125	296/57	190/10	94/31	GCMT
11153442	17.07.08	42.4794	-30.5047	4,5	4,8	42/82/-165	266/16	175/5	70/73	GCMT
12969476	22.09.07	42.8124	-31.866	5,1	5,2	89/51/-111	297/73	194/4	102/16	GCMT
7143768	15.06.05	42.8539	-29.344	4,4	4,8	69/64/-55	26/56	134/12	232/31	ZUR_RMT
13494993	23.03.08	43.1783	-29.1421	4,1	4,8	12/40/-97	148/83	287/5	17/4	GCMT
598169	02.05.82	43.5666	-28.9402	5,3		52/55/-73	10/74	130/8	222/14	HRVD
1143618	03.06.98	43.5754	-29.0113	5,0	5,5	23/42/-116	203/72	311/6	43/17	HRVD
17103712	31.08.11	43.6005	-28.8625	5,3	5,6	21/47/-102	217/82	119/1	29/8	GCMT
17536390	31.08.11	43.6005	-28.8625	5,3	5,6	1/51/-105	215/78	102/5	11/11	GCMT
7071588	27.08.03	43.6161	-28.9045	5,1	5,4	24/50/-106	231/77	125/4	35/13	HRVD
2708602	14.01.02	43.628	-28.709	4,7	5,0	39/72/-83	319/62	123/27	217/7	ZUR_RMT
945880	05.02.96	43.6789	-28.5922	4,9		200/33/-64	225/70	91/14	358/14	HRVD
346281	04.12.90	43.7197	-28.8681	5,2		36/41/-68	43/74	290/6	199/14	HRVD
3759988	13.04.02	43.856	-28.576	3,9	4,4	34/57/-84	323/77	119/12	210/5	ZUR_RMT
11184430	23.08.08	44.3289	-28.1569	4,7	5,0	202/45/-69	195/75	98/2	7/14	GCMT
604161166	23.01.14	44.4146	-28.3914	3,8	4,9	36/61/-55	355/58	101/10	197/30	GCMT
2379216	27.11.01	44.459	-28.181	4,6	5,1	223/68/-59	174/56	291/17	30/29	HRVD
12778999	25.07.07	44.5516	-28.2143	4,6	5,1	14/42/-104	180/80	294/4	25/9	GCMT
602762023	07.04.13	44.58	-28.22	4,4	4,8	16/41/-89	94/86	286/4	195/1	GCMT
1039114	16.05.00	44.669	-28.282	4,6	5,1	46/45/-73	39/78	304/1	213/12	HRVD
1735514	16.05.00	44.669	-28.282	4,6	5,1	15/66/-95	276/69	109/21	17/4	ZUR_RMT
1334466	18.12.98	44.7824	-28.095	4,8	5,4	227/76/-68	164/54	299/28	41/22	HRVD
6687576	05.04.03	44.8395	-28.0857	4,5	4,8	19/30/-83	89/74	283/15	192/4	ZUR_RMT
1763574	21.01.01	44.874	-28.115	4,8	5,4	183/52/-75	147/77	262/6	353/12	HRVD
502666	02.02.86	44.9115	-28.1528	5,0		215/32/-55	231/65	100/17	4/18	HRVD
7378670	03.05.05	44.9316	-28.2079	4,5	4,5	23/25/-87	108/70	292/20	201/1	ZUR_RMT
7381628	20.05.05	44.9395	-28.0229	4,5	4,8	189/65/-85	110/69	275/20	7/5	ZUR_RMT
1763568	20.01.01	44.958	-28.163	4,9	5,2	26/54/-73	345/74	104/8	196/14	ZUR_RMT
1835480	21.01.01	44.981	-28.101	4,3	5,0	9/66/-89	280/69	98/21	188/1	ZUR_RMT
7378284	01.05.05	44.9855	-28.1946	4,5	5,0	27/15/-71	90/59	281/31	188/5	ZUR_RMT
403518	02.05.89	44.9897	-28.0172	5,1		194/64/-73	137/67	271/17	6/16	HRVD
1763570	20.01.01	45.038	-28.074	4,7	4,8	12/50/-90	280/85	102/5	12/0	ZUR_RMT
1763588	21.01.01	45.067	-28.089	4,4	4,8	4/64/-83	290/70	88/19	181/7	ZUR_RMT
403502	02.05.89	45.071	-28.1455	5,3		0/45/-90	180/90	90/0	180/0	HRVD
1763590	21.01.01	45.072	-28.139	4,8	5,3	183/45/-74	178/79	82/1	352/11	HRVD
600889808	18.04.12	45.1213	-28.0931	4,5	4,7	215/55/-64	181/68	286/6	19/21	GCMT
2728135	18.01.02	45.167	-27.877	4,5	4,7	184/30/-83	255/74	89/15	358/3	ZUR_RMT
7188716	21.11.03	45.1901	-28.0074	4,8	5,4	4/44/-99	179/84	281/1	11/6	HRVD
7183425	21.11.03	45.24	-27.9919	4,5	5,0	98/46/-40	79/55	335/10	238/34	ZUR_RMT
7188613	21.11.03	45.24	-27.9919	4,5	5,0	12/32/-99	129/76	288/13	19/5	ZUR_RMT
12649091	06.05.07	45.4411	-27.6986	4,5	5,2	8/42/-89	80/87	277/3	187/1	GCMT
7188784	21.11.03	45.4596	-28.0522	4,6	4,8	14/25/-94	113/69	287/21	18/2	ZUR_RMT
503021	07.02.86	45.4661	-27.9248	5,0		221/63/-41	183/47	279/5	13/42	HRVD
2379187	25.11.01	45.565	-27.814	4,9	5,1	9/59/-93	269/76	102/14	11/3	ZUR_RMT
2708526	11.01.02	45.806	-27.56	4,5	4,7	5/69/-97	264/65	101/24	8/7	ZUR_RMT
583617	26.02.83	45.9045	-27.592	5,0		232/29/-29	227/52	98/27	354/25	HRVD
10389756	19.01.07	45.9805	-27.4834	4,5	4,8	32/61/-61	350/62	102/11	197/25	GCMT
587252	22.12.82	46.0229	-27.5662	5,1		24/55/-72	342/73	101/9	194/15	HRVD
485094	27.10.86	46.0292	-27.6262	5,3		0/29/-100	115/73	278/16	9/5	HRVD
460721	27.08.87	46.1349	-27.5089	4,7		13/45/-90	180/90	103/0	13/0	HRVD

EventID	Date	Latitude	Longitude	mb	Mw	Strike/Dip/Rake	P Az/Pl	T Az/Pl	N Az/Pl	Author
11121506	11.09.06	46.3272	-27.4927	4,9	5,0	183/47/-79	165/82	265/1	356/8	GCMT
13822395	03.10.09	46.368	-27.3681	4,7	4,9	27/43/-82	47/84	291/3	201/6	GCMT
1048921	23.10.97	46.3751	-27.5	5,0	5,5	220/40/-44	212/59	99/13	2/27	HRVD
13822600	06.10.09	46.4252	-27.3291	5,1	4,9	17/77/-52	324/44	79/23	187/37	GCMT
602425794	06.02.13	46.432	-27.45	5,0	5,3	8/45/-103	189/81	287/1	17/9	GCMT
13822435	04.10.09	46.441	-27.3204	4,6	4,8	37/54/-74	356/75	115/7	207/13	GCMT
504423	24.02.86	46.4647	-27.452	4,8		204/57/-56	170/61	271/6	4/28	HRVD
13551367	08.08.09	46.5246	-27.446	4,8	5,1	14/45/-97	195/85	289/0	19/5	GCMT
14791428	30.06.10	46.5306	-27.5512	4,7	4,8	5/48/83	100/3	220/84	10/5	GCMT
295185	09.04.92	46.7235	-27.3854	5,1		181/67/-84	102/67	266/22	358/6	HRVD
2728137	19.01.02	46.775	-27.494	4,6	4,8	48/44/-40	31/56	285/11	188/32	ZUR_RMT
6545055	27.01.03	46.8761	-27.2795	4,7	5,0	17/31/-91	110/76	288/14	18/1	ZUR_RMT
478123	08.12.86	46.9415	-27.4217	5,1		219/31/-50	231/62	100/19	3/19	HRVD
465802	04.05.87	46.9612	-27.4107	5,0		7/34/-85	77/79	273/11	183/3	HRVD
15252302	15.10.10	46.9861	-27.2233	4,9	5,1	5/39/-104	158/79	285/7	16/9	GCMT
16448726	15.10.10	46.9861	-27.2233	4,9	5,1	3/80/-178	227/8	318/6	83/80	GCMT
13813945	19.12.08	47.0134	-27.3007	5,5	5,9	4/39/-83	58/82	269/6	178/3	NEIC
11933759	25.04.07	47.0588	-27.4934	4,9	5,4	1/37/-92	100/82	272/8	2/1	GCMT
8320397	12.04.06	47.0975	-27.4166	4,1	4,9	11/43/-89	88/88	281/2	191/0	HRVD
603812233	18.11.13	47.1003	-27.1921	4,4	4,8	17/53/-77	332/77	98/8	189/10	GCMT
2788992	03.02.02	47.145	-27.356	4,7	5,1	31/20/-64	80/62	280/27	186/9	ZUR_RMT
7236038	17.01.04	47.1709	-27.3979	4,3	4,8	41/18/-27	49/50	261/35	159/16	ZUR_RMT
11123311	07.12.06	47.1865	-27.2788	4,6	5,0	182/53/-80	133/79	265/7	356/8	GCMT
7667398	06.07.05	47.207	-26.2277	4,1	4,6	15/32/-83	83/77	280/13	189/4	ZUR_RMT
11458376	19.11.08	47.2921	-27.4645	4,7	5,2	172/46/-92	38/88	264/1	174/1	GCMT
465105	25.06.87	47.3136	-27.4456	5,4		193/50/-69	168/74	268/3	359/16	HRVD
1800458	24.03.01	47.706	-30.604	4,9	5,2	15/77/95	101/32	292/57	194/5	ZUR_RMT
11706270	27.03.07	47.713	-27.5116	4,4	5,0	20/44/-89	80/89	289/1	199/1	GCMT
7666216	14.06.05	47.7323	-27.7624	4,1	4,5	18/26/-73	74/69	276/20	183/7	ZUR_RMT
3443454	28.09.02	47.764	-27.909	4,6	4,7	4/43/-119	189/70	294/6	26/20	ZUR_RMT
604376687	31.03.14	47.9509	-27.7689	4,4	4,9	15/56/-70	332/71	91/9	184/16	GCMT
2153016	16.10.01	47.985	-27.599	4,5	4,5	156/33/-81	218/77	60/12	329/5	ZUR_RMT
3036443	17.05.02	48.22	-27.786	5,7	5,6	230/76/-17	186/22	277/2	13/68	HRVD
7150769	05.10.03	48.342	-27.9588	4,2	4,6	158/72/-85	75/63	245/27	337/4	ZUR_RMT
8481016	14.06.06	48.6652	-27.9037	4,3	4,9	199/56/-72	153/72	276/10	9/15	HRVD
314246	21.11.91	48.7472	-28.0471	5,1		178/45/-90	180/90	268/0	178/0	HRVD
10698908	14.06.06	48.7817	-27.9192	4,7	4,8	4/35/-98	125/79	280/10	11/5	HRVD
428670	11.08.88	49.1768	-28.375	5,3		163/45/-90	180/90	253/0	163/0	HRVD
11255517	02.09.08	49.1779	-28.3034	4,4	4,9	177/49/-81	140/82	261/4	352/7	GCMT
11505810	19.02.07	49.194	-28.3929	5,1	5,3	183/48/-85	147/85	269/3	359/4	GCMT
1003257	02.07.98	49.2381	-28.9619	4,9	5,1	19/57/55	134/6	234/60	41/29	HRVD
1164157	02.07.98	49.2381	-28.9619	4,9	5,1	180/60/106	258/14	124/70	352/14	HRVD
8939964	30.10.06	49.3249	-28.2776	4,2	4,7	1/49/-80	329/82	83/3	174/8	GCMT
1737896	16.07.00	49.41	-28.511	4,5	4,7	17/23/-78	85/67	278/23	186/5	ZUR_RMT
603503054	30.09.13	49.435	-28.538	5,4	5,5	194/36/-74	229/76	93/10	1/9	GCMT
14280392	27.01.10	49.4531	-28.5573	4,7	4,9	31/49/-70	9/75	107/2	197/15	GCMT
2034685	30.08.01	49.462	-28.511	4,9	5,2	189/15/-72	255/59	85/31	352/4	HRVD
12814267	27.08.07	49.4964	-28.4783	4,4	5,0	6/53/-93	262/82	98/8	7/2	GCMT
10700027	23.08.06	49.6184	-28.5648	4,4	4,8	156/48/-80	128/82	239/3	330/7	HRVD
7333489	22.04.04	49.8757	-28.8806	4,5	4,8	163/63/-97	58/71	257/18	166/6	ZUR_RMT
7333694	23.04.04	49.9004	-28.9145	4,7	5,1	181/58/-80	120/75	263/12	355/9	ZUR_RMT
13213617	06.02.08	50.1095	-28.9333	4,8	5,0	191/47/-74	175/78	270/1	0/12	GCMT

EventID	Date	Latitude	Longitude	mb	Mw	Strike/Dip/Rake	P Az/Pl	T Az/Pl	N Az/Pl	Author
6837448	08.05.03	50.1283	-30.1096	4,8	5,0	181/90/-180	46/0	136/0	180/90	HRVD
3211777	11.06.02	50.14	-29.172	4,6	5,0	169/34/-80	225/78	72/11	341/5	ZUR_RMT
6836580	07.05.03	50.1446	-30.0621	5,2	5,1	3/71/177	227/11	320/15	102/71	HRVD
7373915	20.07.04	50.2017	-29.229	4,7	4,9	200/76/-22	157/25	249/5	349/64	HRVD
14742267	05.06.10	50.3058	-29.1049	4,7	4,8	189/59/-77	131/72	269/13	2/11	GCMT
7072799	29.08.03	50.6209	-28.7147	4,9	5,2	109/52/89	200/7	14/83	110/1	HRVD
7484489	24.03.05	50.6597	-22.8679	4,3	4,5	151/22/-97	253/67	66/23	157/3	ZUR_RMT
7459347	05.01.05	50.9369	-29.821	4,5	4,7	7/35/-64	27/71	258/12	165/15	ZUR_RMT
954391	20.03.96	51.0528	-30.0581	5,0	5,2	187/71/-78	115/62	268/25	3/11	HRVD
953280	14.03.96	51.9742	-30.1716	4,7	5,3	194/68/-64	141/58	264/19	3/24	HRVD